applied optics

Hybrid generation and analysis of vector vortex beams

Sandra Mamani,[1] Ethan Bendau,[1] Jeff Secor,[1] Solyman Ashrafi,[2] Jiufeng J. Tu,[1] and Robert R. Alfano[1,*]

[1]Institute for Ultrafast Spectroscopy and Lasers, Department of Physics, The City College of The City University of New York, 160 Convent Avenue, New York, New York 10031, USA
[2]NxGen Partners, Ross Tower, 500 N. Akard Street, Suite 1820, Dallas, Texas 75201, USA
*Corresponding author: ralfano@ccny.cuny.edu

Received 18 November 2016; revised 13 February 2017; accepted 14 February 2017; posted 14 February 2017 (Doc. ID 280970); published 7 March 2017

A method is described for generating optical vector vortex beams carrying superpositions of orbital angular momentum states by using a tandem application of a spatial light modulator with a vortex retarder. The vortex component has a spatially inhomogeneous phase front that can carry orbital angular momentum, and the vector nature is a spatially inhomogeneous state of polarization in the laser beam profile. The vector vortex beams are characterized experimentally by imaging the beams at points across the focal plane in an astigmatic system using a tilted lens. Mathematical analysis of the Gouy phase shows good agreement with the phase structure obtained in the experimental images. The polarization structure of the vector beam and the orbital angular momentum of the vortex beam are shown to be preserved. © 2017 Optical Society of America

OCIS codes: (050.4865) Optical vortices; (080.1010) Aberrations (global); (260.5430) Polarization.

https://doi.org/10.1364/AO.56.002171

1. INTRODUCTION

Optical vector vortex beams have both helical wavefronts carrying orbital angular momentum (OAM) and special inhomogeneous forms of polarization structure in the spatial beam profile. Vortex beams have a helical wavefront that can be clockwise or counterclockwise, similar to left- and-right handed circularly polarized light, and the vortex beam profile contains an azimuthal phase dependence. Optical vortices have been an active topic of research, as they offer new degrees of freedom of light, and have found applications in fields such as optical trapping [1] and quantum communication [2–10]. A variety of methods can be used to generate a complex beam. These include use of a spatial light modulator (SLM) [11,12], cylindrical lens mode converters [13,14], and even generation directly in the laser cavity [15–18]. In general, these methods generate scalar beams with spatially homogeneous polarization (i.e., linear or circular), while other devices such as q-plates [4,19–21] are capable of generating vector beams with a spatially varying state of polarization. The most common of these forms of polarization are radial and azimuthal polarization [3,4,21], which form an orthogonal basis set from which higher-order modes can be defined, similar to the way that combinations of circular polarization of opposite helicity can define any state of linear polarization and vice versa.

Some of the earlier methods of generating beams with vector and vortex properties used subwavelength patterns and metamaterials to tailor the Pancharatnam–Berry phase [22–24]. A vortex retarder (VR) is a recent technological advancement based on liquid crystal polymer wave plates. The VR acts as a wave plate where the phase imparted onto the beam can be spatially designed across the beam profile. Its pattern is described by a topological charge m, and the value of OAM that it can impart to the light beam is $L = 2m\hbar$, where $\hbar$ is Planck's constant divided by 2π. The VR is capable of generating OAM beams similar to electrically activated liquid crystal q-plates [19,25–27], but the VR does not require electrical input as does the q-plate. The VR mediates a spin-to-orbit conversion of circularly polarized light into light carrying OAM, and the spatially inhomogeneous phase retardation generates a vector beam profile. The ability to generate vector beams versus vortex beams is mutually exclusive with a single VR. The focus of this paper is to describe the generation and analysis of vector vortex beams with arbitrary superposition of total values of OAM using a VR in tandem with a SLM.

2. THEORY

The propagation of a linearly polarized beam through a VR is described through the following Jones matrix calculus.

We consider the input to be a Laguerre–Gaussian (LG) of radial mode $p = 0$ and azimuthal mode ℓ generated by the SLM. The intensity profile generated by the SLM is not a perfect LG mode, but this does not change the general analysis. In the following, ℓ is the topological charge imparted from the SLM and $2m$ is the charge from the VR. The matrix equation for the linearly polarized beam propagating through the VR is

$$E_o e^{-i\ell\phi}\begin{bmatrix}\cos\ 2m\phi & \sin\ 2m\phi\\ \sin\ 2m\phi & -\cos\ 2m\phi\end{bmatrix}\begin{bmatrix}1\\0\end{bmatrix} = E_0 e^{-i\ell\phi}\begin{bmatrix}\cos\ 2m\phi\\ \sin\ 2m\phi\end{bmatrix}, \tag{1}$$

where $E_o = E_o(r, \phi, \ell)$ is the input amplitude function, ϕ is the azimuthal angle in the transverse plane of the beam, the matrix is the Jones matrix of the VR, and the column vector is the input polarization. Equation (1) describes a vector beam of order m, and when $m = 1/2$, it represents a radially polarized mode of OAM $= (\ell \pm 2m)\hbar$. Expanding the polarization vector in orthogonal circular polarization basis vectors and using Euler's identity describes the output as the superposition

$$E = E_0\left(e^{i(2m-\ell)\phi}\begin{bmatrix}1\\ i\end{bmatrix} + e^{-i(2m+\ell)\phi}\begin{bmatrix}1\\ -i\end{bmatrix}\right), \tag{2}$$

which expresses the output vector vortex beam as a superposition of OAM states imparted by the SLM and VR. The analysis for azimuthal polarization follows in a similar fashion. In the following, L describes the total OAM content of the beam, ℓ is the topological charge imparted by the SLM, and $M = 2m$ is that of the VR.

3. EXPERIMENT

A SLM and a VR of topological charge $m = \frac{1}{2}$ are combined to generate vector vortex beams with an arbitrary superposition of total angular momentum. The experimental setup is shown in Fig. 1. A He–Ne laser (632.8 nm) is passed through a single-mode optical fiber (TEM 00 mode) and illuminated onto a SLM's screen, which displays a forked diffraction grating. The first-order diffraction is focused through a 400 μm aperture and then recollimated. A rotatable quarter-wave plate controls the circular polarization into the VR. A 20 cm focal length lens on a rotation axis perpendicular to the optic axis focuses the output beam onto the face of a CCD, where the phase front of the beam is analyzed by this method [28]. In our experiment we rotate the lens to 20° (at this point the beam fully decomposes into another beam, as explained in Section 4) with respect to the beam propagation direction; then the beam profile through the focal length is measured over a distance of 20 cm (for full propagation of the beam) to characterize the phase profile and the astigmatism introduced by the tilted lens. Figure 2 shows the output from the VR with the SLM set to $\ell = 0, -1$, and 1, with the light horizontally polarized with respect to the VR axis (to generate radially polarized light with a superposition of $+1$ and -1). To generate vector beams with higher L values, the SLM displays a forked diffraction grating with a higher number of bifurcations, and the rotating fast-axis distribution of the VR generates radial or azimuthal polarization, depending on the orientation of the beam going into the VR with respect to its axis. For example, vertical polarized light is used to generate azimuthal polarization. Figure 3 shows the analysis of the outcome beams, which is also shown mathematically through Eqs. (1) and (2).

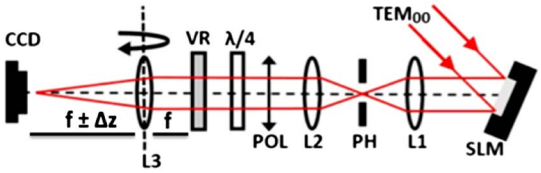

Fig. 1. Optical system for generating and analyzing vortex vector beams. The collimated output of a TEM_{00} single-mode fiber is incident on the SLM at a small angle. Lenses L1 and L2 focus the light through a 400 μm pinhole (PH). A polarizer (POL) and $\lambda/4$ plate control the polarization into the vortex retarder (VR). The third lens L3 ($f = 20$ cm) can rotate about an axis perpendicular to the optic axis, and the imaging CCD translates along the optic axis.

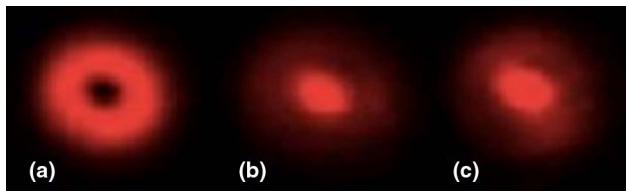

Fig. 2. Images of the beam at the focal plane. The VR contributes an OAM of $M = \pm 1$, while the SLM is set in each case to (a) $\ell = 0$, (b) $\ell = -1$, and (c) $\ell = +1$. The intensity at the center in (b) and (c) follows from the superposition described in Eq. (2).

4. ANALYSIS

The polarization of the output beams is shown in Fig. 3 for different values of $\ell + M$. A polarizer placed before the CCD shows that indeed these beams follow an intensity pattern

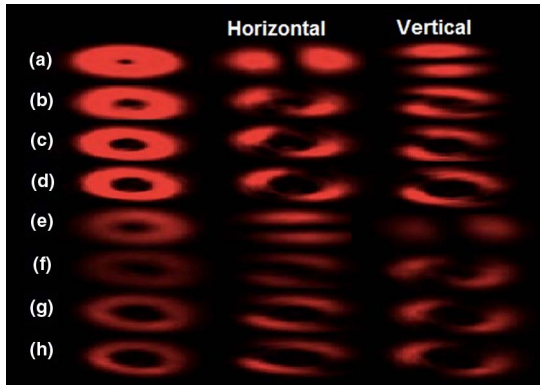

Fig. 3. Polarization analysis of the beam for (a)–(d) radial and (e)–(h) azimuthal polarizations. The VR in all cases contributes $M = \pm 1$ unit of OAM, and the SLM contributes ℓ as follows: (a), (e) $\ell = 0$; (b), (f) $\ell = 2$; (c), (g) $\ell = 3$; (d), (h) $\ell = 4$. The first column is with no analyzer, and the second and third columns are with the analyzer set parallel and perpendicular, respectively, to the input polarization. The variation in the intensities between radial and azimuthal polarizations is due to the orientation of the first polarizer with respect to the fiber output. In principle, the intensity profiles would be the same for equal values of total L. Nonetheless, the azimuthal and radial polarization is preserved with higher OAM values.

expected for radial and azimuthal polarization with higher values of ℓ. (When using a vertical analyzer, the radially polarized beam breaks up into two lobes, one on top of the other, while for azimuthally polarized beam the two lobes are next to each other, or 90° rotated from the radial polarization case. The opposite happens when using a horizontal analyzer.) To measure the phase structure and OAM content of the beam, there are a number of methods including mode sorters [9,29,30], Dammann vortex gratings [31,32], gradually changing period grating [33,34], and astigmatism by a tilted lens [28,35–39]. In this case we used the tilted lens, which is an easily accessible and simple method of phase front analysis. Following the analysis of [28], we note that a LG beam can be expanded as a superposition of Hermite–Gaussian (HG) modes along the x and y axes, and offset by a phase shift of $\frac{\pi}{2}$. As the beam propagates through the focus of the tilted lens, the difference between the complex argument of terms β_1 and β_2 increases and then decreases back to zero, as shown in the following:

$$\beta_j = \left(\frac{kw_j}{2z}\right)^2 + i\frac{k}{2z}, \tag{3}$$

$$\frac{1}{w_j^2} = \frac{1}{w_0^2} + i\frac{k}{2z}\left(1 - \frac{zc_j}{f}\right),$$

$$c_1 = \sec\theta, \qquad c_2 = \cos\theta, \qquad j = t, s,$$

where z is the propagation distance from the tilted lens, $k = \frac{2\pi}{\lambda}$ is the wave vector, w_j is the beam waist at some j position, w_0 is the beam waist at its minimum spot size, w_f is the beam waist at focus, f is the focal length of the lens, θ is the tilt angle, and t and s indicate the tangential or sagittal plane, respectively. The terms β_1 and β_2 describe, in part, the phase shift known as the Gouy phase that a beam obtains as it propagates through the focus. In the astigmatic system, the tangential and sagittal components of the beam experience unequal phase shifts, leading to a short window of distance where the t and s components obtain a relative phase difference near $\frac{\pi}{2}$, which brings the HG terms of the LG expansion back into phase such that the image is a recognizable HG mode. Figure 4 shows the Gouy phase shift calculated from Eq. (3) for the t and s planes, along with the difference between them. This plot shows that the region of maximally clear mode conversion where the two planes have a relative phase shift of nearly $\frac{\pi}{2}$ occurs within 1 cm of the focal

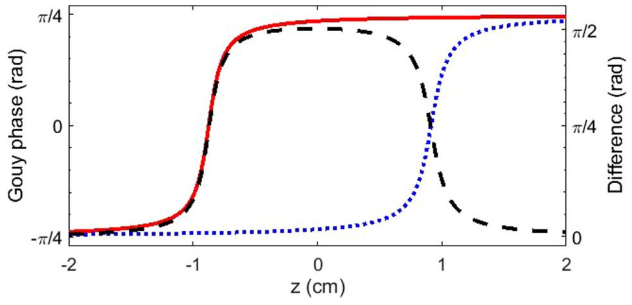

Fig. 4. Theoretical Gouy phase evolution based on Eq. (3) in the sagittal plane (dotted blue curve) and tangential plane (solid red curve). $z = 0$ corresponds to the focus of the lens. The phase difference between the planes (dashed black curve, right axis) shows the plateau corresponding to the region of clearest mode transformation.

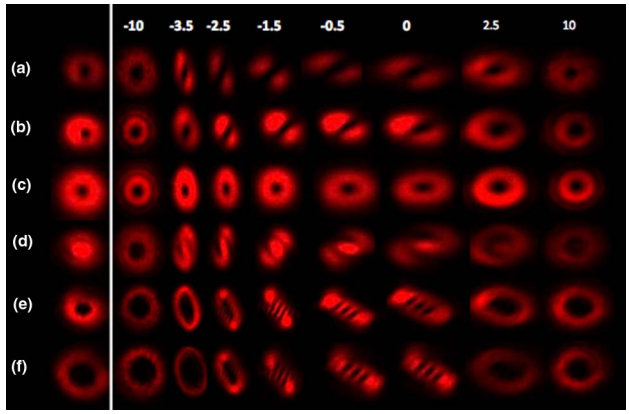

Fig. 5. Images of the beam through the focal region of an astigmatic lens. The first column shows the image at the focus of the lens with no astigmatism. Columns 2–9 show the evolution of the beam profile through the focusing of the tilted lens from $z = -10$ cm to $z = +10$ cm from the focus at $z = 0$. (a) No VR and $\ell = -1$, (b) $\ell = 0$, $M = -1$, (c)–(e) radially polarized $M = \pm 1$ with $\ell = 0$, 1, and −4, (f) azimuthally polarized $M = \pm 1$ with $\ell = -4$.

length of the lens. The number of dark lines between the end nodes indicates the HG mode components of the beam and thus the total OAM value of the vortex wavefront. We use this knowledge to analyze the phase structure of the vortex vector beams shown in Fig. 5. The beam profiles in the focal plane of the lens show the superposition of the HG component modes of the beams. When the VR of $M = 1$ is paired with a vortex beam of $\ell = 1$ generated by the SLM, we expect that the image will be a superposition of both an $L = 0$ and an $L = 2$ beam. Indeed, the image with no tilt is distinctly composed of an outer, lower intensity beam (as intensity decreases with increasing values of L) corresponding to the $L = 2$ component, the vortex of which appears "filled in" by the $L = 0$ component. Similarly, when the VR is paired with a vortex beam of $\ell = -4$ generated by the SLM, we see a larger donut profile compared with lower-order modes, as the ring size scales positively with L. Also, in the focal plane of the tilted lens, we distinctly see the HG profile, including three dark lines between the nodes, corresponding to an $L = -3$ beam. In this case, the profile of the $L = -5$ overlaps with the other mode and the characteristic dark lines are partially obscured by the end node of the $L = -3$ beam.

5. CONCLUSION

A simple method is described for the generation of vortex vector beams composed of an arbitrarily high superposition of OAM states differing by $\Delta L = 2$ using a zero-order half-wave VR in tandem with a SLM. The helical phase of the vortex beam and the complex vector polarization are shown to be preserved when combined in this manner. The ability to control both the polarization and OAM of a beam gives one an efficient means to utilize a greater range of degrees of freedom of these complex beams. This could have applications in new telecommunication schemes, quantum communication, entanglement, and other applications of complex light beams where the higher

degrees of freedom are utilized. The addition of a VR offers a quick method to incorporate vector beam character into vortex beam applications, and the measurement of the phase profile through the focus presents a broader analysis of the tilted lens measurements in relation to the Gouy phase.

Funding. National Science Foundation (NSF) (1464994); Army Research Office (ARO) (W911NF-13-1-0151); Corning Incorporated Foundation (71198-00 10); NxGen (75029-00 01).

Acknowledgment. We thank ARO, NSF (under award NSF-1464994), Corning, and NxGen for partial support of the Complex Light program at CCNY and Dan Nolan for helpful discussion and support of research at IUSL and CCNY. Finally, we thank the reviewers for their efforts to improve the manuscript.

REFERENCES

1. A. D. Kiselev and D. O. Plutenko, "Optical trapping by Laguerre beams: symmetries, stability and equilibria," Phys. Rev. A **94**, 013804 (2016).
2. V. D'Ambrosio, E. Nagali, S. P. Walborn, L. Aolita, S. Slussarenko, L. Marrucci, and F. Sciarrino, "Complete experimental toolbox for alignment-free quantum communication," Nat. Commun. **3**, 961 (2010).
3. G. Milione, T. A. Nguyen, J. Leach, D. A. Nolan, and R. R. Alfano, "Using the nonseparability of vector beams to encode information for optical communication," Opt. Lett. **40**, 4887–4890 (2015).
4. G. Milione, M. P. J. Lavery, H. Huang, Y. Ren, G. Xie, T. A. Nguyen, E. Karimi, L. Marrucci, D. A. Nolan, R. R. Alfano, and A. E. Willner, "4 × 20 Gbit/s mode division multiplexing over free space using vector modes and a *q*-plate (de)multiplexer," Opt. Lett. **40**, 1980–1983 (2015).
5. A. E. Willner, H. Huang, Y. Yan, Y. Ren, N. Ahmed, G. Xie, C. Bao, L. Li, Y. Cao, Z. Zhao, J. Wang, M. P. J. Lavery, M. Tur, S. Ramachandran, A. F. Molisch, N. Ashrafi, and S. Ashrafi, "Optical communications using orbital angular momentum beams," Adv. Opt. Photonics **7**, 66–106 (2015).
6. J. Wang, J. Y. Yang, I. M. Fazal, N. Ahmed, Y. Yan, H. Huang, Y. Ren, Y. Yue, S. Dolinar, M. Tur, and A. E. Willner, "Terabit free-space data transmission employing orbital angular momentum multiplexing," Nat. Photonics **6**, 488–496 (2012).
7. E. Ip, G. Milione, M. J. Li, N. Cvijetic, K. Kanonakis, J. Stone, G. Peng, X. Prieto, C. Montero, V. Moreno, and J. Liñares, "SDM transmission of real-time 10 GbE traffic using commercial SFP + transceivers over 0.5 km elliptical-core few-mode fiber," Opt. Express **23**, 17120–17126 (2015).
8. G. Milione, E. Ip, M. J. Li, J. Stone, G. Peng, and T. Wang, "Mode crosstalk matrix measurement of a 1 km elliptical core few-mode optical fiber," Opt. Lett. **41**, 2755–2758 (2016).
9. H. Huang, G. Milione, M. P. J. Lavery, G. Xie, Y. Ren, Y. Cao, N. Ahmed, T. A. Nguyen, D. A. Nolan, M. J. Li, M. Tur, R. R. Alfano, and A. E. Willner, "Mode division multiplexing using an orbital angular momentum mode sorter and MIMO-DSP over a graded-index few-mode optical fibre," Sci. Rep. **5**, 14931 (2015).
10. G. Milione, D. A. Nolan, and R. R. Alfano, "Determining principal modes in a multimode optical fiber using the mode dependent signal delay method," J. Opt. Soc. Am. B **32**, 143–149 (2015).
11. N. Matsumoto, T. Ando, T. Inoue, Y. Ohtake, N. Fukuchi, and T. Hara, "Generation of high-quality higher-order Laguerre-Gaussian beams using liquid-crystal-on-silicon spatial light modulators," J. Opt. Soc. Am. A **25**, 1642–1651 (2008).
12. N. Cvijetic, G. Milione, E. Ip, and T. Wang, "Detecting lateral motion using light's orbital angular momentum," Sci. Rep. **5**, 15422 (2015).
13. M. J. Padgett and L. Allen, "Orbital angular momentum exchange in cylindrical-lens mode converters," J. Opt. B **4**, S17–S19 (2002).
14. M. J. Padgett and J. Courtial, "Performance of a cylindrical lens mode converter for producing Laguerre–Gaussian laser modes," Opt. Commun. **159**, 13–18 (1999).
15. K. Hinman and J. P. Young, "Intra-cavity generation of Laguerre-Gauss laser beams via a high-loss circular mask," in *Frontiers in Optics 2015*, OSA Technical Digest (Optical Society of America, 2015), paper JW2A.83.
16. D. Naidoo, K. At-Ameur, M. Brunel, and A. Forbes, "Intra-cavity generation of superpositions of Laguerre-Gaussian beams," Appl. Phys. B **106**, 683–690 (2012).
17. A. Hasnaoui and K. Ait-Ameur, "Properties of a laser cavity containing an absorbing ring," Appl. Opt. **49**, 4034–4043 (2010).
18. P. Miao, Z. Zhang, J. Sun, W. Walasik, S. Longhi, N. M. Litchinitser, and L. Feng, "Orbital angular momentum microlaser," Science **353**, 464–467 (2016).
19. S. Slussarenko, A. Murauki, T. Du, V. Chigrinov, L. Marrucci, and E. Santamato, "Tunable liquid crystal q-plates with arbitrary topological charge," Opt. Express **19**, 4085–4090 (2011).
20. L. Yan, P. Gregg, E. Karimi, A. Rubano, L. Marrucci, R. Boyd, and S. Ramachandran, "*Q*-plate enabled spectrally diverse orbital-angular-momentum conversion for STED microscopy: supplementary material," Optica **2**, 900–903 (2015).
21. G. Millione, A. Dudley, T. A. Nguyen, O. Chakraborty, E. Karimi, A. Forbes, and R. A. Alfano, "Measuring the self-healing of the spatially inhomogeneous states of polarization of vector Bessel beams," J. Opt. **17**, 035617 (2015).
22. A. Niv, G. Biener, V. Kleiner, and E. Hasman, "Rotating vectorial vortices produced by space-variant subwavelength gratings," Opt. Lett. **30**, 2933–2935 (2005).
23. W. Chen, W. Han, D. C. Abeysinghe, R. L. Nelson, and Q. Zhan, "Generating cylindrical vector beams with subwavelength concentric metallic gratings fabricated on optical fibers," J. Opt. **13**, 015003 (2010).
24. J. Zeng, J. Gao, T. S. Luk, N. M. Litchinitser, and X. Yang, "Structuring light by concentric-ring patterned magnetic metamaterial cavities," Nano Lett. **15**, 5363–5368 (2015).
25. Y. S. Rumala, G. Milione, T. A. Nguyen, S. Pratavieira, Z. Hossain, D. Nolan, S. Slussarenko, E. Karimi, L. Marrucci, and R. R. Alfano, "Tunable supercontinuum light vector vortex beam generator using a q-plate," Opt. Lett. **38**, 5083–5086 (2013).
26. Y. Rumala, S. Pratavieira, G. Milione, T. A. Nguyen, Z. Hossain, D. Nolan, E. Karimi, S. Slussarenko, L. Marrucci, and R. R. Alfano, "Supercontiuum light vector beam generation with a tunable liquid crystal q-plate," in *Frontiers in Optics 2013*, OSA Technical Digest (Optical Society of America, 2013), paper FTu1F.4.
27. J. A. Davis, N. Hashimoto, M. Kurihara, E. Hurtado, M. Pierce, M. M. Sanchez-Lopez, K. Badham, and I. Moreno, "Analysis of a segmented *q*-plate tunable retarder for the generation of first-order vector beams," Appl. Opt. **54**, 9583–9590 (2015).
28. P. Vaity, J. Banerji, and R. P. Singh, "Measuring the topological charge of an optical vortex by using a tilted convex lens," Phys. Lett. A **377**, 1154–1156 (2013).
29. G. C. G. Berkhout, M. P. J. Lavery, J. Courtial, M. W. Beijersbergen, and M. J. Padgett, "Efficient sorting of orbital angular momentum states of light," Phys. Rev. Lett. **105**, 153601 (2010).
30. M. Mirhosseini, M. Malik, Z. Shi, and R. W. Boyd, "Efficient separation of the orbital angular momentum eigenstates of light," Nat. Commun. **4**, 2781 (2013).
31. N. Zhang, X. C. Yuan, and R. E. Burge, "Extending the detection range of optical vortices by Dammann vortex gratings," Opt. Lett. **35**, 3495–3497 (2010).
32. S. Fu, T. Wang, S. Zhang, and C. Gao, "Integrating 5 × 5 Dammann gratings to detect orbital angular momentum states of beams with the range of −24 to +24," Appl. Opt. **55**, 1514–1517 (2016).
33. K. Dai, C. Gao, L. Zhong, Q. Na, and Q. Wang, "Measuring OAM states of light beams with gradually-changing-period gratings," Opt. Lett. **40**, 562–565 (2015).
34. S. Fu, T. Wang, Y. Gao, and C. Gao, "Diagnostics of the topological charge of optical vortex by a phase-diffractive element," Chin. Opt. Lett. **14**, 080501 (2016).

35. E. Abramochkin and V. Volostnikov, "Beam transformation and non-transformed beams," Opt. Commun. **83**, 123–135 (1991).
36. S. G. Reddy, S. Prabhkar, A. Aadhi, J. Banerji, and R. P. Singh, "Propagation of an arbitrary vortex pain through an astigmatic optical system and determination of its topological charge," J. Opt. Soc. Am. A **31**, 1295–1302 (2014).
37. L. Allen, M. W. Beijersbergen, R. J. C. Spreeuw, and J. P. Woerdman, "Orbital angular momentum of light and the transformation of Laguerre-Gaussian laser modes," Phys. Rev. A **45**, 8185–8189 (1992).
38. A. Y. Bekshaev, M. S. Soskin, and M. V. Vasnetsov, "Optical vortex symmetry breakdown and decomposition of the orbital angular momentum of light beams," J. Opt. Soc. Am. A **20**, 1635–1643 (2003).
39. A. Wada, T. Ohtani, Y. Miyamoto, and M. Takeda, "Propagation analysis of the Laguerre–Gaussian beam with astigmatism," J. Opt. Soc. Am. A **22**, 2746–2755 (2005).

134.74.186.201 {ts '2017-03-05 11:30:40'}